

# Integrating Weather Foundation Model and Satellite to Enable Fine-Grained Solar Irradiance Forecasting

Ziqing Ma\*

maziqing.mzq@alibaba-inc.com  
DAMO Academy, Alibaba Group  
Hangzhou, Zhejiang, China

Kai Ying\*

yingkai.ying@alibaba-inc.com  
DAMO Academy, Alibaba Group  
Hangzhou, Zhejiang, China  
College of Computer Science,  
Zhejiang University of Technology  
Hangzhou, Zhejiang, China

Xinyue Gu\*

guxinyue.gxy@alibaba-inc.com  
DAMO Academy, Alibaba Group  
Hangzhou, Zhejiang, China

Tian Zhou\*

tian.zt@alibaba-inc.com  
DAMO Academy, Alibaba Group  
Hangzhou, Zhejiang, China

Tianyu Zhu\*

yunrui.zty@alibaba-inc.com  
DAMO Academy, Alibaba Group  
Hangzhou, Zhejiang, China

Haifan Zhang

zhanghaifan.zhf@alibaba-inc.com  
DAMO Academy, Alibaba Group  
Hangzhou, Zhejiang, China

Peisong Niu

niupeisong.nps@alibaba-inc.com  
DAMO Academy, Alibaba Group  
Hangzhou, Zhejiang, China

Wang Zheng

zhengwang@zjut.edu.cn  
College of Computer Science,  
Zhejiang University of Technology  
Hangzhou, Zhejiang, China

Cong Bai

congbai@zjut.edu.cn  
College of Computer Science,  
Zhejiang University of Technology  
Hangzhou, Zhejiang, China

Liang Sun

liang.sun@alibaba-inc.com  
DAMO Academy, Alibaba Group  
Bellevue, USA

## Abstract

Accurate day-ahead solar irradiance forecasting is essential for integrating solar energy into the power grid. However, it remains challenging due to the pronounced diurnal cycle and inherently complex cloud dynamics. Current methods either lack fine-scale resolution (e.g., numerical weather prediction, weather foundation models) or degrade at longer lead times (e.g., satellite extrapolation). We propose Baguan-solar, a two-stage multimodal framework that fuses forecasts from Baguan, a global weather foundation model, with high-resolution geostationary satellite imagery to produce 24-hour irradiance forecasts at kilometer scale. Its decoupled two-stage design first forecasts day-night continuous intermediates (e.g., cloud cover) and then infers irradiance, while its modality fusion jointly preserves fine-scale cloud structures from satellite and large-scale constraints from Baguan forecasts. Evaluated over East Asia using CLDAS as ground truth, Baguan-solar outperforms strong baselines (including ECMWF IFS, vanilla Baguan, and SolarSeer), reducing

RMSE by 16.08% and better resolving cloud-induced transients. An operational deployment of Baguan-solar has supported solar power forecasting in an eastern province in China, since July 2025. Our code is accessible at <https://github.com/DAMO-DI-ML/Baguan-solar.git>.

## CCS Concepts

• **Computing methodologies** → **Supervised learning by regression**.

## Keywords

Solar irradiance forecasting, Weather foundation models, Multimodal fusion, Satellite imagery, Swin Transformer.

## ACM Reference Format:

Ziqing Ma, Kai Ying, Xinyue Gu, Tian Zhou, Tianyu Zhu, Haifan Zhang, Peisong Niu, Wang Zheng, Cong Bai, and Liang Sun. 2018. Integrating Weather Foundation Model and Satellite to Enable Fine-Grained Solar Irradiance Forecasting. In *Proceedings of Make sure to enter the correct conference title from your rights confirmation email (Conference acronym 'XX)*. ACM, New York, NY, USA, 12 pages. <https://doi.org/XXXXXXXX.XXXXXXX>

## 1 Introduction

The inherent variability of solar irradiance, driven largely by cloud dynamics, presents a major challenge to integrating solar power into the electricity grid, impacting both its stability and operational efficiency [31]. Accurate day-ahead (24 h) forecasting of surface

\*Authors contributed equally to this work.

Permission to make digital or hard copies of all or part of this work for personal or classroom use is granted without fee provided that copies are not made or distributed for profit or commercial advantage and that copies bear this notice and the full citation on the first page. Copyrights for components of this work owned by others than the author(s) must be honored. Abstracting with credit is permitted. To copy otherwise, or republish, to post on servers or to redistribute to lists, requires prior specific permission and/or a fee. Request permissions from [permissions@acm.org](mailto:permissions@acm.org).

Conference acronym 'XX, June 03–05, 2018, Woodstock, NY

© 2018 Copyright held by the owner/author(s). Publication rights licensed to ACM.

ACM ISBN 978-1-4503-XXXX-X/2018/06

<https://doi.org/XXXXXXXX.XXXXXXX>

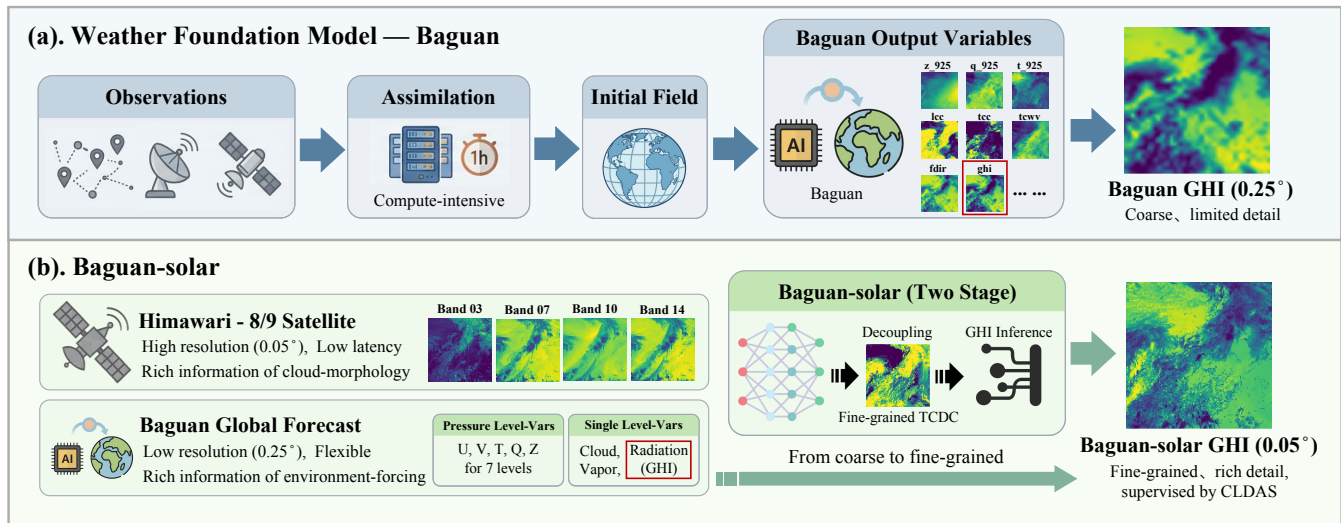


Figure 1: From coarse Baguan forecasts to fine-grained GHI: the Baguan-solar overall framework.

solar irradiance, typically quantified as Global Horizontal Irradiance (GHI), is therefore essential to enable the large-scale, reliable, and cost-effective integration of solar energy into modern power systems [10].

Despite its importance, day-ahead GHI forecasting remains difficult for two fundamental reasons. First, GHI exhibits a pronounced diurnal cycle: it is strictly zero at night and increases rapidly after sunrise, introducing strong discontinuities around day–night transitions [31]. Second, accurate forecasts must simultaneously capture fine-scale cloud morphology (which drives sharp local irradiance fluctuations) and remain skillful at longer lead times, where cloud motion errors accumulate and cloud evolution involves formation and dissipation rather than pure advection [21].

Currently, mainstream operational and research solutions for GHI forecasting can be broadly grouped into three categories: (i) physics-based numerical weather prediction (NWP), (ii) data-driven weather foundation models (WFMs), and (iii) satellite-based extrapolation methods. NWP models solve the governing physical equations of atmospheric dynamics and radiation, offering strong physical consistency and reliable long-horizon predictability. However, they are computationally expensive and often struggle to resolve the fine-scale, rapidly evolving cloud processes that dominate local irradiance variability [1, 19]. In addition, they also suffer from the so called “spin-up” problem, making it often inaccurate in the early-hour prediction [30].

Recent advances in WFMs present a promising alternative to conventional NWP systems. WFMs such as Pangu-Weather [3], FuXi [7], GraphCast [17], and Baguan [24] have demonstrated forecasting skill surpassing NWP models at medium ranges, while drastically reducing computational expense. These models learn to predict the evolution of global atmospheric fields typically at  $0.25^\circ$ . However, current WFMs remain suboptimal for solar energy applications due to two key limitations. First, they are primarily trained to optimize conventional meteorological variables (e.g., wind, temperature, humidity), yet many lack outputs for irradiance

or cloud-specific parameters that are essential for solar forecasting, as summarized in Appendix Table 4. Second, their native spatial resolution is too coarse to adequately resolve mesoscale cloud structures. Furthermore, increasing the spatial resolution leads to a dramatic growth in computational cost, making high-resolution global WFMs impractical in real-world deployment [22].

In parallel, satellite extrapolation based methods have made compelling progress in high-resolution solar nowcasting [1, 4, 21]. Geostationary platforms, such as Himawari-8/9 [2], provide multi-spectral imagery at kilometer-scale resolution and minute-scale cadence, offering a rich description of cloud morphology, cloud-top temperature, and moisture structure. Models like SolarSeer [1] leverage such satellite imagery to forecast GHI over large domains (e.g., CONUS) at 5 km resolution, achieving substantial speed-ups while narrowing the error gap. At longer lead times (12–24 h), satellite-only methods become a mere extrapolation problem, ignoring atmospheric dynamics in different layers and leading to degraded performance.

These observations highlight a critical gap: existing approaches either (i) provide physically rich but coarse and computationally expensive forecasts (NWP, WFMs), or (ii) offer high spatial resolution and low latency but rely solely on satellite extrapolation, which limits longer-horizon skill. However, a seamless integration of WFMs with satellite observations for solar irradiance forecasting remains a recognized challenge in the field. To bridge this gap, we propose Baguan-solar, a two-stage, multimodal framework that integrates WFMs forecasts with satellite imagery for fine-grained solar irradiance forecasting. The overall framework is illustrated in Figure 1. To handle the pronounced diurnal cycle, in which GHI changes abruptly around sunrise and sunset, Baguan-solar employs a decoupled two-stage design. The first stage targets intermediate variables like total cloud cover and future satellite imagery, ensuring consistent modeling across day and night. These outputs then serve as inputs to the second stage, which infers GHI by combining them with clear-sky GHI and meteorological context. To jointly preserve fine-scale cloud morphology while maintaining

day-ahead skill, Baguan-solar further adopts a modality-fusion design that leverages high-resolution satellite observations to capture local cloud structures and uses Baguan forecasts [24] to provide large-scale dynamical and thermodynamical constraints that guide longer-horizon cloud evolution.

Baguan-solar is comprehensively evaluated over East Asia using the China Meteorological Administration’s Land Data Assimilation System (CLDAS) [27] as ground truth. CLDAS provides a spatially and temporally consistent analysis by assimilating dense surface observations and satellite retrievals, making it a superior reference for GHI over East Asia compared with reanalysis datasets such as ERA5. Evaluated on CLDAS, Baguan-solar outperforms a range of baselines, including vanilla Baguan [24], ECMWF Integrated Forecasting System (IFS), SolarSeer [1]. Under our operational setting, Baguan-solar reduces GHI RMSE by approximately 16.08% relative to the strongest baseline, while substantially improving the representation of rapid irradiance transients associated with passing clouds. In summary, the contributions of this work are fourfold:

- (1) We propose Baguan-solar, a multimodal fusion framework that integrates Baguan forecasts with geostationary satellite imagery to produce fine-grained day-ahead (24 h) GHI forecasts.
- (2) We design a decoupled two-stage Swin Transformer that first forecasts day–night continuous cloud-related intermediates and then infers GHI.
- (3) We conduct comprehensive experiments over East Asia using CLDAS as ground truth, demonstrating that Baguan-solar consistently outperforms strong baselines (including Baguan, ECMWF IFS, and satellite-based methods).
- (4) We demonstrate operational deployment of Baguan-solar in an online forecasting system, where it runs hourly using the latest Baguan forecasts and satellite data as input to support real-world solar power forecasting.

## 2 Related Work

### 2.1 WFMs for Irradiance Forecasting

WFMs have progressed rapidly in recent years. Existing WFMs can be broadly categorized into two architectural paradigms: graph-based and transformer-based models. Graph-based approaches [17, 18] naturally accommodate Earth’s geometry and enabling flexible spatial discretization. In contrast, transformer-based approaches [3, 6, 7, 23] typically tokenize gridded meteorological fields and leverage attention mechanisms for spatiotemporal modeling. Beyond architectural choices, Baguan [24] adopts a pre-training–fine-tuning pipeline to mitigate overfitting under limited real-world data. However, most existing WFMs [3, 6, 7, 16–18, 23] do not natively support solar irradiance forecasting. To the best of our knowledge, only Baguan and FuXi-2.0 [32] provide irradiance-related outputs. Moreover, although WFMs like Baguan produce surface irradiance fields, their predictions are not specifically optimized for solar-energy applications and remain restricted to a coarse  $0.25^\circ$  spatial resolution.

### 2.2 From WFMs to Downstream Irradiance Products

Recent studies demonstrate the potential of building downstream irradiance forecasting applications on top of WFMs. Huang et al.

propose FuXi-RTM [13], which couples FuXi [7] with a fixed radiative transfer model to enforce radiative-transfer consistency during training. Similarly, NVIDIA Earth-2 [5] integrates the FourCastNet SFNO forecasting model with dedicated radiation diagnostic modules to generate global multi-day solar irradiance forecasts. In industry, GraphCast [17] forecasts have also been used as multi-variable meteorological inputs for power-market applications [8, 29]. However, these advances remain limited by coarse resolution, as they focus on model-side adaptations without leveraging satellite observations to enhance fine-grained forecasting.

### 2.3 Satellite-based Irradiance Forecasting

Complementary to WFM-based irradiance products, satellite imagery provides high-frequency, high-resolution observations of cloud evolution and has become an effective auxiliary modality for day-ahead solar irradiance forecasting. Boussif et al. propose CrossViViT [4], which improves site-level irradiance prediction by incorporating geostationary satellite imagery. Extending to multi-site settings, Schubnel et al. develop SolarCrossFormer [26], which couples satellite patches with station networks via graph-based cross-attention. For solar power forecasting, Ma et al. present FusionSF [21], a tri-modal framework that integrates NWP outputs and satellite images, using vector quantization to align heterogeneous modalities. However, most multimodal methods remain limited to site-specific forecasts and lack scalable, gridded outputs for broader applications. To bridge this gap, Bai et al. propose SolarSeer [1], an end-to-end model that uses historical satellite observations to forecast cloud cover and irradiance at 5 km resolution, offering faster inference and lower RMSE than HRRR. However, its reliance on satellite observations alone limits accuracy at longer lead times.

## 3 Multimodal Datasets

This section describes the multimodal datasets used in our study, as summarized in Table 1, including geostationary satellite observations (Himawari), regional analysis fields from CLDAS, global reanalysis data (ERA5), and global WFM forecasts. Although these datasets have different spatial coverages, all data are cropped to their common spatial intersection for subsequent analyses.

### 3.1 Satellite Observations

We utilize multi-spectral imagery from the Himawari-8/9 geostationary satellites, operated by the Japan Meteorological Agency (JMA) [2]. These satellites provide full-disk observations over the Asia-Pacific region at 10-minute intervals, with spatial resolutions of 0.5–2 km depending on the channel. The visible, near-infrared, and thermal infrared bands capture critical information on cloud optical properties, aerosol loading, and atmospheric moisture. Given its low latency (<30 minutes), this data stream serves as a timely observational constraint for short-term solar irradiance prediction. Himawari-8/9 observations from the Advanced Himawari Imager (AHI) include 13 spectral bands. The complete set of AHI bands, together with their central wavelengths and typical applications, is summarized in Table 5. Following SolarSeer [1], we focus on four AHI bands: B03, B07, B10, and B14, with central wavelengths of 0.64, 3.9, 7.3, and 11.2  $\mu\text{m}$ , respectively.

**Table 1: Summary of datasets used in our study. The reported spatial resolution refers to the effective resolution used in our experiments after interpolating the original products.**

Dataset	Spatial Resolution	Coverage	Channels	Usage
Himawari	0.05°	Asia-Pacific	Band 0.64, 3.9, 7.3, and 11.2 $\mu\text{m}$	Input during training and inference
CLDAS	0.05°	East Asia	SSRD, TCDC	Training target
ERA5	0.25°	Global	U, V, T, Q, Z, TCC, SSRD, etc.	Input during training
Baguan forecast	0.25°	Global	U, V, T, Q, Z, TCC, SSRD, etc.	Input during inference

### 3.2 CLDAS Analysis Fields

The CLDAS [27] provides hourly, near-real-time land surface analysis over East Asia ( $0^\circ$ – $65^\circ\text{N}$ ,  $60^\circ$ – $160^\circ\text{E}$ ) at an effective resolution of  $0.01^\circ$ . For consistency with our model grid, we interpolate the CLDAS fields to  $0.05^\circ$  resolution. CLDAS integrates surface observations from over 30,000 automatic weather stations, FengYun satellite retrievals, radar-based precipitation estimates, and background fields from CMA’s numerical models through a statistical blending framework. We use CLDAS-derived GHI, computed from downward surface shortwave radiation (SSRD), as the target variable for model training and evaluation, where  $\text{GHI} (\text{W m}^{-2}) = \text{SSRD} (\text{J m}^{-2})/3600$ . In addition, we include TCDC (total cloud cover) from CLDAS as an auxiliary predictor to provide complementary information on cloudiness conditions.

### 3.3 ERA5 Dataset

ERA5 [11], produced by the European Centre for Medium-Range Weather Forecasts (ECMWF), is a widely used global atmospheric reanalysis that provides comprehensive hourly estimates of a wide range of meteorological variables at a resolution of  $0.25^\circ$ . During the training stage, ERA5 supplies the large-scale meteorological context essential for learning the spatiotemporal dynamics of irradiance-relevant variables. In the inference stage, however, the ERA5 fields are replaced by real-time forecasts generated by Baguan [24], enabling fully operational forecasting. Additionally, while ERA5 can serve as a reference (“ground truth”) for GHI, it is inherently less accurate and coarser than higher-fidelity observational products such as CLDAS.

### 3.4 Baguan Global Forecasts

We incorporate operational forecasts from Baguan [24], a state-of-the-art data-driven global weather prediction system trained on ERA5 dataset. Baguan provides  $0.25^\circ$ -resolution forecasts of key atmospheric variables, including GHI, at hourly lead times up to 14 days. Within our framework, during inference, Baguan supplies the large-scale meteorological context and a coarse predictive signal for GHI, which we further refine using high-resolution satellite observations. In addition, Baguan serves as a WFM baseline, as it directly produces GHI forecasts at  $0.25^\circ$  resolution.

## 4 Baguan-solar Framework

As illustrated in Figure 2, Baguan-solar contains two stages: (i) *cloud evolution modeling* and (ii) *irradiance inference modeling*. Stage 1 explicitly forecasts the future 24 h cloud cover and satellite images

by fusing historical 6 h multi-spectral geostationary satellite observations and 30 h Baguan weather forecasts (spanning both the past 6 h and the subsequent 24 h). Stage 2 then infers the future 24 h GHI forecast by combining Stage 1 cloud-aware outputs with clear-sky GHI and radiation-relevant Baguan variables. Specifically, clear-sky GHI is estimated by the Ineichen–Perez model and is a deterministic function of longitude, latitude, and time (see Appendix A.4). Both stages are implemented with Swin Transformer [20] backbones to capture multi-scale spatial structures efficiently while preserving high-resolution outputs via patch embedding and patch recovery.

### 4.1 Stage 1: Cloud Evolution Modeling.

Accurate GHI forecasting critically depends on predicting cloud evolution, since clouds dominate radiative attenuation and introduce strong spatiotemporal nonlinearity. Thus, Stage 1 is formulated as an explicit cloud-field forecasting task. Specifically, it leverages two complementary inputs: (i) historical satellite observations  $\mathbf{X}_{t-5:t}^{\text{sat}} \in \mathbb{R}^{6 \times 4 \times H_{\text{sat}} \times W_{\text{sat}}}$ , where the four spectral channels are defined in Section 3.1; and (ii) Baguan weather forecasts  $\mathbf{X}_{t-5:t+24}^{\text{bg}} \in \mathbb{R}^{30 \times C_1 \times H_{\text{bg}} \times W_{\text{bg}}}$ . We select a total of  $C_1 = 39$  Baguan channels, including moisture, cloud state, thermodynamic, and dynamical conditions (see Appendix Table 6). All Baguan variables are interpolated to the satellite grid.

Architecturally, Stage 1 uses two Swin Transformer encoders to disentangle cloud morphology and atmospheric forcing. We first project satellite observations and Baguan forecast fields into patch tokens via modality-specific patch embeddings  $\phi_{\text{sat}}(\cdot)$  and  $\phi_{\text{bg}}(\cdot)$ , and then feed them into a *Cloud-Morphology Encoder* and a *Cloud-Environment Encoder*, respectively. Each encoder consists of 8 stacked Swin Transformer blocks with residual connections, layer normalization and multi head attention. We use a patch size of  $8 \times 8$ , a window size of 16, an embedding dimension of 256, and 2 attention heads in each transformer layer. The Cloud-Morphology Encoder extracts multi-scale cloud textures and boundary cues from satellite imagery to produce  $\mathbf{Z}^{\text{sat}}$ , while the Cloud-Environment Encoder encodes the interpolated Baguan variables to capture dynamical and thermodynamical conditions, yielding  $\mathbf{Z}^{\text{bg}}$ . We then apply cross-attention to inject environmental guidance into the satellite representation, and concatenate the enhanced satellite tokens with the Baguan tokens to form a fused representation  $\mathbf{Z}^{\text{fused}}$ :

$$\mathbf{Z}^{\text{sat}} = \text{Enc}_{\text{sat}}(\phi_{\text{sat}}(\mathbf{X}^{\text{sat}})), \quad \mathbf{Z}^{\text{bg}} = \text{Enc}_{\text{bg}}(\phi_{\text{bg}}(\mathbf{X}^{\text{bg}})), \quad (1)$$

$$\mathbf{Z}^{\text{fused}} = \text{cat}(\mathbf{Z}^{\text{sat}} + \text{Attn}(\mathbf{Z}^{\text{sat}}W_Q, \mathbf{Z}^{\text{bg}}W_K, \mathbf{Z}^{\text{bg}}W_V), \mathbf{Z}^{\text{bg}}). \quad (2)$$

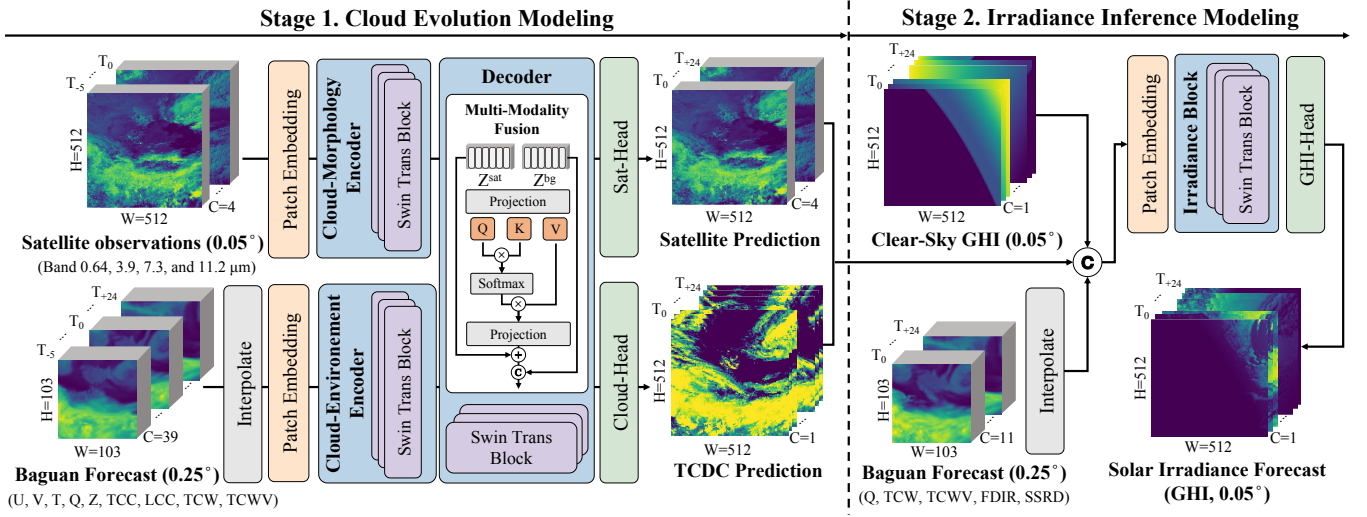


**Figure 2: Baguan-solar model architecture.** Baguan-solar uses a two-stage Swin Transformer framework that fuses Himawari satellite observations with Baguan forecasts to first predict cloud-related intermediates (satellite fields and TCDC) and then infer 24 h high-resolution GHI.

Finally,  $Z^{\text{fused}}$  is processed by a shared Swin Transformer decoder followed by two task-specific heads to jointly generate the day-ahead total cloud cover forecast  $\hat{Y}_{t+1:t+T_{\text{out}}}^{\text{TCDC}}$  and future satellite predictions  $\hat{Y}_{t+1:t+T_{\text{out}}}^{\text{sat}}$ .

$$[\hat{Y}_{t+1:t+T_{\text{out}}}^{\text{TCDC}}, \hat{Y}_{t+1:t+T_{\text{out}}}^{\text{sat}}] = \text{Dec}(Z^{\text{fused}}). \quad (3)$$

## 4.2 Stage 2: Irradiance Inference Modeling.

Stage 2 infers irradiance by integrating the cloud-aware intermediate outputs from Stage 1 with additional meteorological and physical priors. Specifically, we construct the Stage 2 input by concatenating the Stage 1 predictions  $\hat{Y}_{t+1:t+24}^{\text{TCDC}}$  and  $\hat{Y}_{t+1:t+24}^{\text{sat}}$ , together with the clear-sky GHI  $X_{t+1:t+24}^{\text{clear-sky}}$  and Baguan forecast variables  $X_{t+1:t+24}^{\text{bg}} \in \mathbb{R}^{T_{\text{out}} \times C_2 \times H_s \times W_s}$  with  $C_2 = 11$  radiation-relevant channels. The concatenated tensor is patch-embedded and processed by a Swin Transformer backbone with 8 stacked Swin blocks, patch size  $P=8$ , and hidden dimension  $D=256$ . A Solar Irradiance head then performs patch recovery to restore the original spatial resolution and outputs multi-step GHI forecasts:

$$\hat{Y}^{\text{ghi}} = \text{Irr}(\text{cat}(X^{\text{clear-sky}}, X^{\text{bg}}, \hat{Y}^{\text{TCDC}}, \hat{Y}^{\text{sat}})). \quad (4)$$

We train the two-stage model in an end-to-end manner with a weighted multi-task objective over three prediction targets. We use mean squared error (MSE) as the loss function for all tasks:

$$\mathcal{L} = \lambda_{\text{sat}} \mathcal{L}_{\text{sat}} + \lambda_{\text{TCDC}} \mathcal{L}_{\text{TCDC}} + \lambda_{\text{ghi}} \mathcal{L}_{\text{ghi}}. \quad (5)$$

where  $\lambda_{\text{sat}} = 1$ ,  $\lambda_{\text{TCDC}} = 0.5$ , and  $\lambda_{\text{ghi}} = 1$  in all experiments.

## 4.3 Implementation & Evaluation

The multimodal dataset from 2022–2024 is used for model development and is split into training and validation subsets at a 0.9:0.1 ratio. Data from 2025 are reserved exclusively for testing to provide an independent evaluation. All inputs are cropped to a  $512 \times 512$  pixel

domain covering East Asia. Baguan-solar is trained on 8 NVIDIA A100 GPUs with a batch size of 4. The training of Baguan-solar uses the scheduler-free optimizer [9], which removes the need for an explicit learning-rate schedule while maintaining stable convergence. The complete set of model hyperparameters is provided in Appendix A.3.

To assess the quality of GHI forecasts, we adopt the root mean squared error (RMSE) as the primary metric, consistent with prior studies [1, 24, 25]. RMSE is computed as:

$$\text{RMSE} = \sqrt{\frac{1}{n} \sum_{i=1}^n (y_i - \hat{y}_i)^2}, \quad (6)$$

where  $n$  denotes the number of samples in the test set, and  $y_i$  and  $\hat{y}_i$  are the observed and predicted GHI values. Smaller RMSE values correspond to more accurate forecasts.

## 5 Experiments

### 5.1 Benchmarking on CLDAS

**5.1.1 Baselines and Experimental Setup.** We evaluate Baguan-solar against the following established benchmarks:

#### Operational Weather Models:

- **Baguan** [24]: An operational weather foundation model designed for renewable energy, providing irradiance-relevant parameters at  $0.25^\circ$  resolution.
- **EC IFS**: ECMWF (EC) Integrated Forecasting System (IFS) is a high-resolution ( $0.1^\circ$ ) NWP system that directly outputs surface solar radiation downward (SSRD), serving as a robust benchmark.

#### Satellite-based Models:

- **SolarSeer** [1]: A state-of-the-art, satellite-based nowcasting model, retrained our dataset for a region-fair evaluation.

**Table 2: Benchmark comparison (RMSE) for solar irradiance forecasting (GHI  $W m^{-2}$ ) over East Asia in 2025, evaluated for forecasts initialized at 00:00 and 12:00 UTC. Results are reported at lead times of 1 h, 2 h, 3 h, 6 h, 12 h, and 24 h, as well as the average RMSE over 1–24 h (Avg.).**

Model	Type	Inputs	RMSE ( $W m^{-2}$ )						
			Avg.	1 h	2 h	3 h	6 h	12 h	24 h
Mean	Statistical	None	83.89	–	–	–	–	–	–
Clear-sky	Statistical	None	113.54	–	–	–	–	–	–
Baguan [24]	weather foundation model	Gridded initial field	58.17	49.53	58.57	65.50	77.98	37.86	37.13
EC IFS	NWP	Gridded initial field	54.46	47.48	59.86	70.65	72.23	37.59	36.50
SolarSeer [1]	Extrapolation-based	Satellite	53.09	36.07	51.40	64.40	68.75	33.14	35.47
Two-stage Unet	Extrapolation-based	Satellite	59.10	47.03	60.32	72.15	74.79	39.10	41.78
Two-stage Swin	Extrapolation-based	Satellite	49.89	32.74	46.77	59.23	65.33	31.46	33.51
Baguan-solar	Multimodal	ERA5 & Satellite	41.21	29.99	43.52	55.04	57.66	24.80	24.20
<b>Baguan-solar (oper.)</b>	Multimodal	Baguan forecasts & Satellite	41.87	30.31	43.64	55.34	57.98	25.18	25.04

- **Two-stage U-Net:** Our two-stage U-Net baseline, built following SolarSeer’s two-stage design.
- **Two-stage Swin:** Our two-stage Swin Transformer baseline, also built following SolarSeer’s two-stage design.

#### Statistical Baselines:

- **Mean:** Predicts the historical average GHI for each hour from the training period (2022–2024).
- **Clear-sky:** Estimates the theoretical GHI under cloud-free conditions based on spatiotemporal coordinates.

Both weather model forecasts are bilinearly interpolated to  $0.05^\circ$  for a consistent comparison. All models are evaluated on a common test set comprising data from the year 2025.

**5.1.2 Overall Performance Comparison.** We evaluate Baguan-solar against a comprehensive set of baselines. As summarized in Table 2, the operational Baguan-solar achieves the best performance, reducing the average RMSE by 16.08% compared to the strongest baseline, the Two-stage Swin, and reducing RMSE by 28.02% relative to the Baguan forecasts. The extrapolation-based methods, especially SolarSeer and Two-stage Swin, show clear advantages over operational weather models. This performance gap stems primarily from their training on high-resolution ( $0.05^\circ$ ) CLDAS data. The finer spatial resolution allows these models to better capture local GHI variability, leading to systematic gains over coarser-resolution approaches such as Baguan at  $0.25^\circ$ . We further evaluate two variants of Baguan-solar. The idealized variant uses ERA5 reanalysis as input, which assumes perfect knowledge of future atmospheric conditions and is not operationally feasible. The operational variant instead uses Baguan forecasts as input, thereby emulating real-time deployment through reforecast experiments. The results show that the idealized version slightly outperforms the operational version, but the gap is small, suggesting that Baguan’s short-term weather forecasts are highly accurate and closely approximate actual atmospheric conditions and introduce only limited degradation in downstream GHI prediction.

**5.1.3 Lead-time-dependent Forecast Skill.** Figure 3 shows how the RMSE of GHI forecasts varies with lead time from 1 to 24 h, comparing Baguan-solar with EC IFS, Baguan [24], and SolarSeer [1].

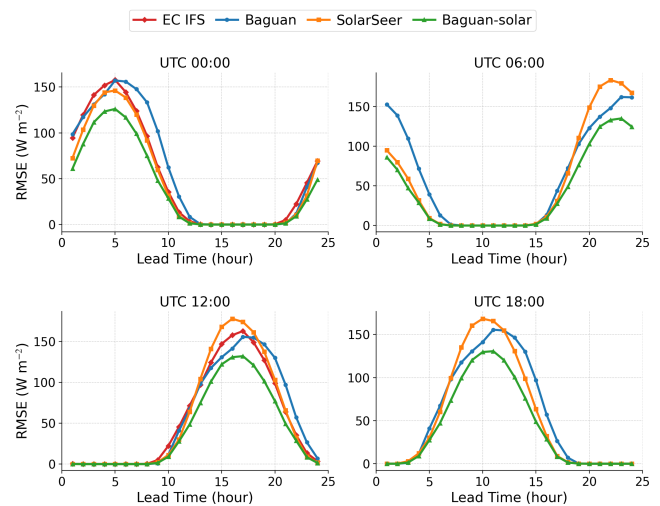


**Figure 3: RMSE of GHI forecasts as a function of lead time (1–24 h) for four initialization times (UTC 00:00, 06:00, 12:00, and 18:00), evaluated over a  $512 \times 512$  gridded domain.**

Across all initialization times (UTC 00:00, 06:00, 12:00, and 18:00), Baguan-solar consistently achieves the lowest errors at every lead time. In addition, a pronounced diurnal cycle is observed in the error curves: errors increase during local daytime, peaking around midday when GHI magnitude is highest, and decrease toward nighttime. During night hours, when GHI is effectively zero, RMSE approaches zero for all methods, reflecting the negligible forecasting uncertainty under no-sun conditions. We also observe that SolarSeer, as an extrapolation-based model, degrades markedly with increasing lead time, consistent with the accumulation of cloud-motion errors and the lack of large-scale dynamical constraints.

## 5.2 Ablation Studies

In this section, we compare variants of Baguan-solar to quantify the modality contributions and stage-wise decoupling. As shown in Table 3, our ablation studies reveal several key insights. Removing Baguan forecasts significantly increases the average RMSE by

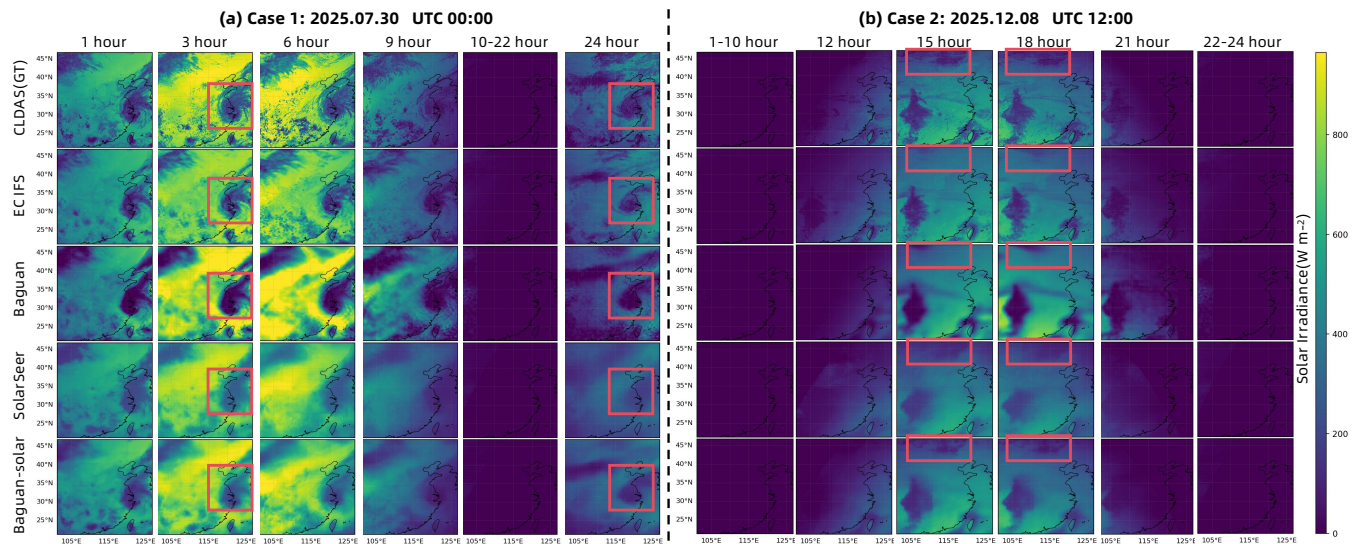


Figure 4: Qualitative comparison of GHI forecast fields for two representative cases initialized at UTC 00:00 and 12:00.

Table 3: Ablation studies on modality contributions and stage-wise decoupling in Baguan-solar. "Only S1" means forecasting GHI and TCDC in a single stage, and then using Clear-sky GHI for post-processing to mask out the night. Results are reported at lead times of 1 h, 2 h, 3 h, 6 h, 12 h, and 24 h, as well as the average RMSE over 1–24 h (Avg.).

Exp. (setting)	RMSE ( $\text{W m}^{-2}$ )						
	Avg.	1 h	2 h	3 h	6 h	12 h	24 h
<b>Baguan-solar (S1+S2)</b>	41.87	30.31	43.64	55.34	57.98	25.18	25.04
w/o Baguan	49.89	32.74	46.77	59.23	65.33	31.46	33.51
w/o satellite	42.66	37.35	49.54	59.36	59.03	25.05	24.60
Baguan-solar (Only S1)	45.50	32.34	44.86	56.38	59.73	35.86	28.92
w/o TCDC	48.30	35.21	47.30	58.37	61.87	41.00	32.62

19.15%. The disparity persists across all lead times, especially at longer lead times, with RMSE increasing by 25.18% at 12 h and 33.82% at 24 h, where the satellite-only extrapolation struggles to capture cloud formation or dissipation. By contrast, Baguan forecasts provide thermodynamic and dynamical conditions that better constrain the evolution of cloud fields, leading to accurate GHI forecasts at longer lead times. Removing satellite increases the average RMSE by 1.88%, while the short-term error increase substantially by 23.22% at 1 h and 13.5% at 2 h. This result emphasizes the role of satellite imagery in capturing fine-scale cloud morphology and boundary motion. In addition, simplifying the two-stage framework to single-stage increases the average RMSE by 8.67%, and further removing TCDC supervision increases it by 15.36%. These results indicate that decoupling cloud evolution provide a physically grounded intermediate constraint that makes GHI variations attributable to forecast cloud occurrence and motion, thereby improving physical consistency.

### 5.3 Qualitative Results

We present two representative cases for qualitative evaluation. The first case (on 2025.07.30) features an organized vortex over East Asia, forming a distinct pattern that low-GHI core surrounded by higher GHI. The Second case (on 2025.12.08), for a typical winter day, features a distinct low-GHI belt over North East Asia. Across both cases, EC IFS follows the overall structure reasonably well but tends to under-suppress the low-GHI core with narrow range and sharp boundaries. Baguan exhibits a systematic bright bias in both cases. SolarSeer is consistently over-smoothed, blurring cloud-band boundaries and gradients. In particular, it fails to retain the vortex-related signature at 24 h in the first case. In contrast, Baguan-solar provides the most balanced reconstruction in both morphology and amplitude. It captures fine-scale structures and transitions for short-term forecast. Although performance degrades with increasing lead time, it still retains the reasonable intensity and spatial extent compared to the other methods.

### 5.4 Modality Importance Analysis

To justify our two-stage design and the inclusion of multimodal data, we use Integrated Gradients (IG) [28] to quantify how much each input modality, satellite versus ERA5 (or Baguan forecasts), contributes to RMSE reduction across lead times 1–24 h. The analysis is performed over 2400 samples and 24 different initialization hours, ensuring robustness to diurnal cycles and variability across initialization times. The feature importance in Figure 5 reveals a clear temporal dynamics: the satellite input contributes significantly (10-31%) to RMSE at short lead times (1–6 h), but it rapidly drops after 6 h and is ultimately below 5% by 24 h. In contrast, ERA5's contribution starts high (68.1%) and steadily increases to over 95% at 24 h.

This pattern justifies two key aspects of our design. First, it highlights the need for including ERA5 (or Baguan forecasts) during training. Although high-resolution satellite data can extrapolate

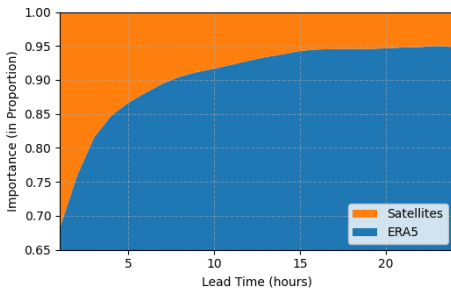


**Figure 5: Importance of ERA5 vs Satellites across lead times.**

well and shine in the nowcasting of GHI, meteorological fields provide essential large-scale dynamical and thermodynamical information to achieve skillful day-ahead forecasts. The finding also coincides with the ablation study in Table 3 and the GHI forecast results in Figure 3. Second, it validates the rationale for the architecture that decouples the forecasting problem into two physically grounded subtasks. Stage 1 is designed to handle the time-varying subtask by learning to dynamically weigh satellite and meteorological inputs according to the forecast horizon, avoiding the degeneration of pure extrapolation. This specialization allows Stage 1 to model difficult cloud evolution under shifting modality dominance as a standalone task. Stage 2 then focuses on the more stable transformation from predicted clouds to GHI, relying only on physical priors such as clear-sky GHI. By separating these concerns, our architecture reduces overall learning difficulty and improves forecast skill across all lead times.

## 6 Deployment

### 6.1 Operational Deployment in East China

Since July 2025, Baguan-solar has been deployed online to support operational solar power forecasting in an eastern province in China, which has the highest solar power capacity of 918.4 GW among all provinces. It is co-deployed with the Baguan weather forecasting system and shares a similar operational pipeline: Baguan is executed four times per day (UTC 00:00, 06:00, 12:00, and 18:00) and produces weather forecasts with lead times up to 14 days. Each time, it takes 0.5 h for Baguan to perform inference on two GPUs. On the other hand, the four AHI bands (B03, B07, B10, and B14) imagery data from Himawari-8/9 geostationary satellites are collected every 10 minutes. Building on the latest available Baguan outputs and satellite data, Baguan-solar runs at a higher frequency (hourly) to provide 24 h high-resolution GHI forecasts, offering a faster but less dynamically constrained view of the evolving atmosphere. The weather forecasts, including the GHI forecasts, are provided to the downstream applications, such as solar power forecasting model and electric load forecasting models [33].

### 6.2 Operational Verification with Pyranometer Sites

We collect GHI measurements from 246 sites equipped with pyranometers in this province and use these in-situ observations to verify Baguan-solar forecasts. Although the previous section uses the CLDAS reanalysis data as the reference due to its fine spatial resolution, pyranometers in these sites provide a more direct

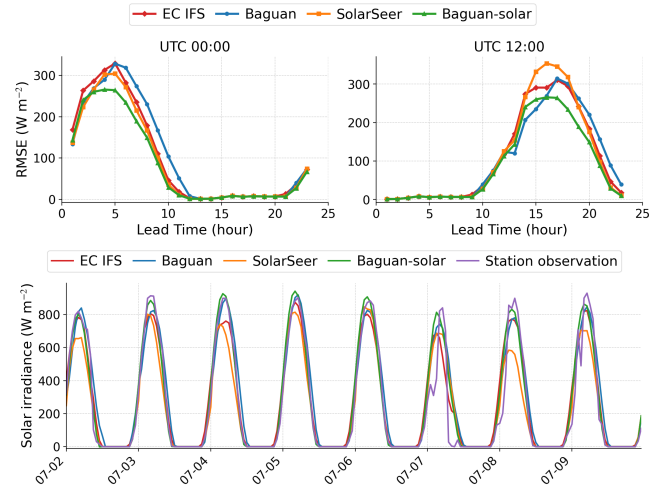


**Figure 6: (Top) RMSE of GHI forecasts as a function of lead time (1–24 h) for two initialization times (UTC 00:00 and 12:00), averaged over 246 sites. (Bottom) Visualization of GHI forecasts for one photovoltaic site over a one-week period.**

and accurate measure of surface GHI and therefore constitute a stricter benchmark for operational validation. To further assess which gridded product better matches the observations, we compute the averaged RMSE between the site measurements and the ERA5/CLDAS fields interpolated to the station locations. ERA5 yields a higher RMSE (77.85) than CLDAS (66.69), indicating that CLDAS provides a more reliable gridded reference over our study region; this also supports our choice of CLDAS as the ground truth for model training and evaluation.

Figure 6 (top) illustrates the RMSE of GHI forecasts for Baguan-solar and other baselines. It shows that Baguan-solar consistently achieves the lowest average errors across all initialization times. SolarSeer, as an extrapolation-based model, degrades remarkably with increasing lead time, with the most pronounced deterioration in the 12–24 h range for the UTC 12:00 initialization. EC IFS and Baguan exhibit similar overall performance; however, Baguan tends to perform worse in the afternoon. In the one-week case study at the photovoltaic site in July 2025 (Figure 6 (bottom)), Baguan-solar shows closer agreement with the site observations than the baseline forecasts, capturing the peak irradiance and the overall temporal variability more accurately.

## 7 Conclusion and Future Work

We presented Baguan-solar, a two-stage model that fuses weather foundation model forecasts and satellite imagery to deliver accurate, fine-grained ( $0.05^\circ$ ) day-ahead solar irradiance predictions. In evaluations, our model surpasses strong baselines (EC IFS, Baguan, and SolarSeer) not only in overall accuracy but also in tracking rapid irradiance changes caused by clouds. It has been in operational use in China since 2025.

Future work includes extending the system globally using multi-satellite data, incorporating uncertainty quantification via ensemble methods, and exploring end-to-end co-training with upstream weather foundation models for improved physical consistency.

## References

- [1] Mingliang Bai, Zuliang Fang, Shengyu Tao, Siqi Xiang, Jiang Bian, Yanfei Xiang, Pengcheng Zhao, Weixin Jin, Jonathan A. Weyn, Haiyu Dong, Bin Zhang, Hongyu Sun, Kit Thambiratnam, Qi Zhang, Hongbin Sun, Xuan Zhang, and Qiuwei Wu. 2025. Ultrafast 24-h solar irradiance forecasts outperform numerical weather predictions across the USA. *Cell Reports Physical Science* 6, 12 (2025), 102996. <https://doi.org/10.1016/j.xcrp.2025.102996>
- [2] Kotaro BESSHO, Kenji DATE, Masahiro HAYASHI, Akio IKEDA, Takahito IMAI, Hidekazu INOUE, Yukihiro KUMAGAI, Takuya MIYAKAWA, Hidehiko MURATA, Tomoo OHNO, Arata OKUYAMA, Ryo OYAMA, Yukio SASAKI, Yoshio SHIMAZU, Kazuki SHIMOJI, Yasuhiko SUMIDA, Masuo SUZUKI, Hidetaka TANIGUCHI, Hiroaki TSUCHIYAMA, Daisaku UESAWA, Hironobu YOKOTA, and Ryo YOSHIDA. 2016. An Introduction to Himawari-8/9 mdash; Japan rsquo;s New-Generation Geostationary Meteorological Satellites. *Journal of the Meteorological Society of Japan. Ser. II* 94, 2 (2016), 151–183. <https://doi.org/10.2151/jmsj.2016-009>
- [3] Kaifeng Bi, Lingxi Xie, Hengheng Zhang, Xin Chen, Xiaotao Gu, and Qi Tian. 2023. Accurate medium-range global weather forecasting with 3D neural networks. *Nature* 619, 7970 (2023), 533–538.
- [4] Oussama Boussif, Ghait Boukachab, Dan Assouline, Stefano Massaroli, Tianle Yuan, Loubna Benabbou, and Yoshua Bengio. 2023. Improving “day-ahead” Solar Irradiance Time Series Forecasting by Leveraging Spatio-Temporal Context. In *Advances in Neural Information Processing Systems 36: Annual Conference on Neural Information Processing Systems 2023, NeurIPS 2023, New Orleans, LA, USA, December 10 - 16, 2023*, Alice Oh, Tristan Naumann, Amir Globerson, Kate Saenko, Moritz Hardt, and Sergey Levine (Eds.). <http://papers.nips.cc/paper/2023/hash/070a57c5ef1e58cc90201b11d369b3c2-Abstract-Conference.html>
- [5] Alberto Carpentieri, Jussi Leinonen, Jeff Adie, Boris Bonev, Doris Folini, and Farah Hariri. 2024. Data-driven Surface Solar Irradiance Estimation using Neural Operators at Global Scale. *arXiv preprint arXiv:2411.08843* (2024).
- [6] Kang Chen, Tao Han, Junchao Gong, Lei Bai, Fenghua Ling, Jing-Jia Luo, Xi Chen, Leiming Ma, Tianning Zhang, Rui Su, et al. 2023. Fengwu: Pushing the skillful global medium-range weather forecast beyond 10 days lead. *arXiv preprint arXiv:2304.02948* (2023).
- [7] Lei Chen, Xiaohui Zhong, Feng Zhang, Yuan Cheng, Yinghui Xu, Yuan Qi, and Hao Li. 2023. FuXi: a cascade machine learning forecasting system for 15-day global weather forecast. *npj Climate and Atmospheric Science* 6, 1 (2023), 190. <https://doi.org/10.1038/s41612-023-00512-1>
- [8] Cale Colony and Razan Andigani. 2024. Solarcast-ML: Per Node GraphCast Extension for Solar Energy Production. *arXiv preprint arXiv:2406.13559* (2024).
- [9] Aaron Defazio, Xingyu Yang, Harsh Mehta, Konstantin Mishchenko, Ahmed Khaled, and Ashok Cutkosky. 2024. The Road Less Scheduled. *arXiv:2405.15682* [cs.LG]
- [10] Michael Emmanuel, Kate Doubleday, Burcin Kadir, Marija Marković, and Bri-Mathias Hodge. 2020. A review of power system planning and operational models for flexibility assessment in high solar energy penetration scenarios. *Solar Energy* 210 (2020), 169–180. <https://doi.org/10.1016/j.solener.2020.07.017> Special Issue on Grid Integration.
- [11] Hans Hersbach, Bill Bell, Paul Berrisford, Shoji Hirahara, András Horányi, Joaquín Muñoz-Sabater, Julien Nicolas, Carole Peubey, Raluca Radu, Dinand Schepers, et al. 2020. The ERA5 global reanalysis. *Quarterly Journal of the Royal Meteorological Society* 146, 730 (2020), 1999–2049.
- [12] William F Holmgren, Clifford W Hansen, and Mark A Mikofski. 2018. pvlib python: A python package for modeling solar energy systems. *Journal of Open Source Software* 3, 29 (2018), 884.
- [13] Qiusheng Huang, Xiaohui Zhong, Xu Fan, Lei Chen, and Hao Li. 2025. FuXi-RTM: A Physics-Guided Prediction Framework with Radiative Transfer Modeling. *CoRR* abs/2503.19940 (2025). <https://doi.org/10.48550/ARXIV.2503.19940> arXiv:2503.19940
- [14] Pierre Ineichen and Richard Perez. 2002. A new airmass independent formulation for the Linke turbidity coefficient. *Solar Energy* 73, 3 (2002), 151–157.
- [15] Japan Meteorological Agency and Meteorological Satellite Center. [n. d.]. Utilization of Meteorological Satellite Data in Cloud Analysis. MSC Technical Note (Special Issue). <https://www.data.jma.go.jp/mscweb/technotes/UtilizationMetSatData.pdf> Accessed: 2026-01-27.
- [16] Thorsten Kurth, Shashank Subramanian, Peter Harrington, Jaideep Pathak, Morteza Mardani, David Hall, Andrea Miele, Karthik Kashinath, and Anima Anandkumar. 2023. FourCastNet: Accelerating Global High-Resolution Weather Forecasting Using Adaptive Fourier Neural Operators. In *Proceedings of the Platform for Advanced Scientific Computing Conference, PASC 2023, Davos, Switzerland, June 26-28, 2023*, Axel Huebel, Cristina Silvano, and Timothy Robinson (Eds.). ACM, 13:1–13:11. <https://doi.org/10.1145/3592979.3593412>
- [17] Remi Lam, Alvaro Sanchez-Gonzalez, Matthew Willson, Peter Wirmberger, Meire Fortunato, Ferran Alet, Suman Ravuri, Timo Ewalds, Zach Eaton-Rosen, Weihua Hu, Alexander Merose, Stephan Hoyer, George Holland, Oriol Vinyals, Jacklynn Stott, Alexander Pritzel, Shakir Mohamed, and Peter Battaglia. 2023. Learning skillful medium-range global weather forecasting. *Science* 382, 6677 (2023), 1416–1421. <https://doi.org/10.1126/science.adid2336> arXiv:https://www.science.org/doi/pdf/10.1126/science.adid2336
- [18] Simon Lang, Mihai Alexe, Matthew Chantry, Jesper Dramsch, Florian Pinault, Baudouin Raoult, Mariana CA Clare, Christian Lessig, Michael Maier-Gerber, Linus Magnusson, et al. 2024. AIFS–ECMWF’s data-driven forecasting system. *arXiv preprint arXiv:2406.01465* (2024).
- [19] Francisco JL Lima, Fernando R Martins, Enio B Pereira, Elke Lorenz, and Detlev Heinemann. 2016. Forecast for surface solar irradiance at the Brazilian Northeastern region using NWP model and artificial neural networks. *Renewable Energy* 87 (2016), 807–818.
- [20] Ze Liu, Yutong Lin, Yue Cao, Han Hu, Yixuan Wei, Zheng Zhang, Stephen Lin, and Baining Guo. 2021. Swin Transformer: Hierarchical Vision Transformer using Shifted Windows. In *2021 IEEE/CVF International Conference on Computer Vision, ICCV 2021, Montreal, QC, Canada, October 10-17, 2021*. IEEE, 9992–10002. <https://doi.org/10.1109/ICCV48922.2021.00986>
- [21] Ziqing Ma, Wenwei Wang, Tian Zhou, Chao Chen, Bingqing Peng, Liang Sun, and Rong Jin. 2024. FusionSF: Fuse Heterogeneous Modalities in a Vector Quantized Framework for Robust Solar Power Forecasting. In *Proceedings of the 30th ACM SIGKDD Conference on Knowledge Discovery and Data Mining, KDD 2024, Barcelona, Spain, August 25-29, 2024*, Ricardo Baeza-Yates and Francesco Bonchi (Eds.). ACM, 5532–5543. <https://doi.org/10.1145/3637528.3671509>
- [22] S Karthik Mukkavilli, Daniel Salles Civitarese, Johannes Schmude, Johannes Jakubik, Anne Jones, Nam Nguyen, Christopher Phillips, Sujit Roy, Shradha Singh, Campbell Watson, et al. 2023. Ai foundation models for weather and climate: Applications, design, and implementation. *arXiv preprint arXiv:2309.10808* (2023).
- [23] Tung Nguyen, Johannes Brandstetter, Ashish Kapoor, Jayesh K. Gupta, and Aditya Grover. 2023. ClimateX: A foundation model for weather and climate. In *International Conference on Machine Learning*. <https://api.semanticscholar.org/CorpusID:256231457>
- [24] Peisong Niu, Ziqing Ma, Tian Zhou, Weiqi Chen, Lefei Shen, Rong Jin, and Liang Sun. 2025. Utilizing Strategic Pre-training to Reduce Overfitting: Baguan - A Pre-trained Weather Forecasting Model. In *Proceedings of the 31st ACM SIGKDD Conference on Knowledge Discovery and Data Mining, V.2, KDD 2025, Toronto ON, Canada, August 3-7, 2025*, Luiza Antonie, Jian Pei, Xiaohui Yu, Flavio Chierichetti, Hady W. Lauw, Yizhou Sun, and Srinivasan Parthasarathy (Eds.). ACM, 2186–2197. <https://doi.org/10.1145/3711896.3737178>
- [25] Stephan Rasp, Stephan Hoyer, Alexander Merose, Ian Langmore, Peter Battaglia, Tyler Russel, Alvaro Sanchez-Gonzalez, Vivian Yang, Rob Carver, Shreya Agrawal, Matthew Chantry, Zied Ben Boualleague, Peter Dueben, Carla Bromberg, Jared Sisk, Luke Barrington, Aaron Bell, and Fei Sha. 2024. WeatherBench 2: A benchmark for the next generation of data-driven global weather models. *arXiv:2308.15560* [physics.ao-ph] <https://arxiv.org/abs/2308.15560>
- [26] Baptiste Schubnel, Jelena Simeunović, Corentin Tissier, Pierre-Jean Alet, and Rafael E Carrillo. 2025. SolarCrossFormer: Improving day-ahead Solar Irradiance Forecasting by Integrating Satellite Imagery and Ground Sensors. *IEEE Transactions on Sustainable Energy* (2025).
- [27] Chunxiang Shi, Lipeng Jiang, Tao Zhang, Dongbin Zhang, Bin Xu, Xiao Liang, and Chen Zhu. 2013. China Land Data Assimilation System (CLDAS) Research and Operation. In *6th WMO Symposium on Data Assimilation*. [https://www.cscamm.umd.edu/programs/das6/program/Posters/abs/Fp13-Shi\\_Chunxiang.pdf](https://www.cscamm.umd.edu/programs/das6/program/Posters/abs/Fp13-Shi_Chunxiang.pdf) Accessed: 2026-01-27.
- [28] Mukund Sundararajan, Ankur Taly, and Qiqi Yan. 2017. Axiomatic Attribution for Deep Networks. In *Proceedings of the 34th International Conference on Machine Learning (Proceedings of Machine Learning Research, Vol. 70)*, Doina Precup and Yee Whye Teh (Eds.). PMLR, 3319–3328. <https://proceedings.mlr.press/v70/sundararajan17a.html>
- [29] Jie Wang, Wenping Qin, Ruipeng Lu, Wenbo Zhang, Haixiao Zhu, and Anting Zhao. 2024. Short-term PV power forecasting system Based on GraphCast Weather Forecasting Model. In *2024 IEEE 8th Conference on Energy Internet and Energy System Integration (EI2)*. IEEE, 5331–5335.
- [30] James L Warner, Jon Petch, Chris J Short, and Caroline Bain. 2023. Assessing the impact of a NWP warm-start system on model spin-up over tropical Africa. *Quarterly Journal of the Royal Meteorological Society* 149, 751 (2023), 621–636.
- [31] Dazhi Yang, Wenting Wang, Christian A. Gueymard, Tao Hong, Jan Kleissl, Jing Huang, Marc J. Perez, Richard Perez, Jamie M. Bright, Xiang’ao Xia, Dennis van der Meer, and Ian Marius Peters. 2022. A review of solar forecasting, its dependence on atmospheric sciences and implications for grid integration: Towards carbon neutrality. *Renewable and Sustainable Energy Reviews* 161 (2022), 112348. <https://doi.org/10.1016/j.rser.2022.112348>
- [32] Xiaohui Zhong, Lei Chen, Xu Fan, Wenxu Qian, Jun Liu, and Hao Li. 2024. FuXi-2.0: Advancing machine learning weather forecasting model for practical applications. *CoRR* abs/2409.07188 (2024). <https://doi.org/10.48550/ARXIV.2409.07188> arXiv:2409.07188
- [33] Zhaoyang Zhu, Weiqi Chen, Rui Xia, Tian Zhou, Peisong Niu, Bingqing Peng, Wenwei Wang, Hengbo Liu, Ziqing Ma, Qingsong Wen, et al. 2023. eForecast: Unifying electricity forecasting with robust, flexible, and explainable machine learning algorithms. In *Proceedings of the AAAI Conference on Artificial Intelligence*, Vol. 37. 15630–15638.

## A Appendix

### A.1 Limitations of weather foundation models

Table 4 highlights a key gap in current weather foundation models (WFMs): despite their strong performance in general meteorological forecasting, large-scale AI models that explicitly predict cloud cover or solar irradiance remain largely unavailable. Baguan-solar is designed to bridge this gap by extending WFMs toward cloud-aware, day-ahead solar irradiance forecasting.

### A.2 Himawari-8/9 Satellite Data

Table 5 summarizes the 16 spectral bands of the Himawari-8/9 Advanced Himawari Imager (AHI), including their center wavelengths, band types (visible, near-infrared, and infrared), and typical meteorological applications. These channels provide complementary information on cloud amount and texture in the visible range, cloud phase and microphysics in the near-infrared, and cloud-top temperature/height as well as water-vapor structure in the infrared. As described by JMA/MSC (2024) [15], Band 3 (0.64  $\mu\text{m}$ ) measures reflected visible solar radiation and supports true-color composites as well as daytime identification of low clouds and fog. Band 7 (3.9  $\mu\text{m}$ ) senses emitted terrestrial radiation and includes a substantial reflected solar component during daytime; at night, it supports hotspot detection and fog/low-cloud identification via the Band 7–Band 13 brightness temperature difference. Band 10 (7.3  $\mu\text{m}$ ) is a water vapor channel primarily sensitive to mid-tropospheric moisture and can also respond to volcanic  $\text{SO}_2$ . Band 14 (11.2  $\mu\text{m}$ ) is a longwave infrared window channel used for cloud imaging and cloud-top characterization, and it can support surface temperature applications under clear-sky conditions.

### A.3 Hyperparameter details

Baguan-solar uses a two-stage Swin Transformer design. The following list summarizes the hyperparameters used for Baguan-solar.

```

image_size: [512, 512]
patch_size: [8, 8]
window_size: 16
embed_dim: 256
num_heads: [2]
patch_norm: True
drop_path_rate: 0.1
mlp_ratio: 4
qkv_bias: True
EnvEncoderSwinNet:
  in_chans: 1170,
  out_chans: 256,
  depths: [8]
SateEncoderSwinNet:
  in_chans: 24,
  out_chans: 256,
  depths: [8]
MultiDecoderSwinNet_Stage1:
  in_chans: 512,
  out_chans: 120,
  depths: [2]
MultiDecoderSwinNet_Stage2:
  in_chans: 17,
  out_chans: 1,

```

depths: [8]

Listing 1: Hyperparameters of Baguan-solar.

### A.4 Fast Vectorized Clear-Sky GHI Computation

Clear-sky global horizontal irradiance (GHI) provides an upper bound of surface irradiance under cloud-free conditions and is widely used as a physics-based prior for solar forecasting. In this work, we adopt the Ineichen–Perez clear-sky model [14] (as implemented in `pvlib` [12]) but re-implement the critical steps using a lightweight, vectorized NumPy routine to enable high-throughput gridded computation.

Our forecasting pipeline requires clear-sky GHI on a dense spatial grid of size  $512 \times 512$  for each time stamp. The `pvlib` library is primarily designed for site-based (per-location) clear-sky computations, necessitating an outer loop over grid cells for grid-wide evaluation. A direct call to `pvlib.clearsky.ineichen` introduces substantial per-point overhead, taking roughly 4 minutes per time step on a  $512 \times 512$  grid with the standard `pvlib` pipeline.

To eliminate this bottleneck, we implement a streamlined clear-sky routine that (i) computes the solar zenith angle using a compact approximation inspired by the NREL Solar Position Algorithm (SPA), and (ii) rewrites the `pvlib.clearsky.ineichen` computation with fully vectorized NumPy broadcasting, allowing latitude, longitude, and elevation to be provided as 2D arrays and yielding clear-sky GHI over the entire raster in a single pass. On a  $512 \times 512$  grid, this reduces the wall-clock time from 4 minutes to 1 second per time step (a  $\sim 240\times$  speedup), while preserving the original physical assumptions and keeping the numerical discrepancy within  $<1\%$ . The Ineichen–Perez clear-sky GHI is computed as follows:

Given the solar zenith angle  $z$  (degrees; determined by longitude, latitude, and time), site elevation  $h$  (meters), Linke turbidity  $T_L$  (dimensionless), day of year DOY, and air mass AM, the Ineichen–Perez clear-sky GHI  $I_{\text{clear}}$  is computed as:

$$I_{\text{clear}} = c_{g1} I_0 \cos(z) \exp\left(-c_{g2} \text{AM} [f_{h1} + f_{h2} (T_L - 1)]\right) \exp(0.01 \text{AM}^{1.8}), \quad (7)$$

where  $I_0$  is the extraterrestrial irradiance (top-of-atmosphere normal irradiance), approximated by:

$$I_0 = 1367.7 \times \left(1 + 0.033 \times \cos\left(\frac{2\pi}{365} \times \text{DOY}\right)\right). \quad (8)$$

The elevation-dependent coefficients are:

$$c_{g1} = 5.09 \times 10^{-5} h + 0.868, \quad (9)$$

$$c_{g2} = 3.92 \times 10^{-5} h + 0.0387, \quad (10)$$

$$f_{h1} = \exp(-h/8000), \quad (11)$$

$$f_{h2} = \exp(-h/1250). \quad (12)$$

Air mass AM is computed from  $z$  using a Kasten–Young–type approximation:

$$\text{AM} = \frac{1}{\cos(z)}. \quad (13)$$

**Table 4: Comparison of representative weather foundation models and solar irradiance forecasting methods, including their inputs/outputs, resolution, region, and whether irradiance-related variables are explicitly modeled.**

Model	Input Variable	Output Variable	Spatial Resolution	Region	Accuracy	Irradiance-related Variable
Graphcast [17]	U10, V10, T2M, MSLP, TP, U, V, Q, Z, T, W	U10, V10, T2M, MSLP, TP, U, V, Q, Z, T, W	0.25°	Global	beats EC IFS	×
Pangu-Weather [3]	U10, V10, T2M, MSLP, U, V, Q, Z, T	U10, V10, T2M, MSLP, U, V, Q, Z, T	0.25°	Global	beats EC IFS	×
Fengwu [6]	U10, V10, T2M, MSLP, U, V, Q, Z, T	U10, V10, T2M, MSLP, U, V, Q, Z, T	0.25°	Global	beats EC IFS	×
Fuxi [7]	U10, V10, T2M, MSLP, TP, U, V, Q, Z, T	U10, V10, T2M, MSLP, TP, U, V, Q, Z, T	0.25°	Global	beats EC IFS	×
Baguan	U10, U100, V10, V100, T2M, MSLP, TP, TCC, LCC, FDIR, SSRD, TCW, TCWV, TP, SP, U, V, Q, Z, T	U10, U100, V10, V100, T2M, MSLP, TP, TCC, LCC, TCW, TCWV, TP, SP, <b>FDIR, SSRD</b> , U, V, Q, Z, T	0.25°	Global	beats EC IFS	✓
SolarSeer [1]	Satellite	<b>SSRD</b>	<b>0.05°</b>	the CONUS	beats HRRR	✓
<b>Baguan-solar</b>	Satellite & Baguan forecasts	<b>SSRD</b>	<b>0.05°</b>	China	beats all baselines	✓

**Table 5: Himawari-8/9 (AHI) spectral bands and typical applications.**

Band	Center wavelength ( $\mu\text{m}$ )	Type	Typical applications
B01	0.47	Visible	Aerosol/land–ocean contrast; thin cloud (daytime)
B02	0.51	Visible	Green band; true-color composition (daytime)
<b>B03</b>	0.64	Visible	Cloud/scene detail; cloud amount (daytime)
B04	0.86	NIR	Vegetation/reflectance; cloud phase aid
B05	1.6	NIR	Cloud phase (ice vs. water); snow–cloud separation; hotspot aid
B06	2.3	NIR	Cloud microphysics (particle size); hotspot aid
<b>B07</b>	3.9	IR (SWIR)	Night fog/low cloud; fires/hotspots; cloud-top temperature support
B08	6.2	IR (WV)	Upper-tropospheric water vapor; jet/upper-level dynamics
B09	6.9	IR (WV)	Mid-level water vapor; moisture structure
<b>B10</b>	7.3	IR (WV)	Lower-level water vapor; dry intrusion/convection environment
B11	8.6	IR	Cloud phase/microphysics; ash/SO <sub>2</sub> discrimination aid
B12	9.6	IR (O <sub>3</sub> )	Ozone absorption; stratospheric influence; deep convection top features
B13	10.4	IR window	Primary cloud-top brightness temperature; cloud-top height proxy
<b>B14</b>	11.2	IR window	Split-window combinations for fog/dust/ash; microphysics
B15	12.4	IR window	Split-window for fog/low cloud, dust; SST/LST retrieval support
B16	13.3	IR (CO <sub>2</sub> )	CO <sub>2</sub> slicing for cloud-top height; thin cirrus detection

In our experiments, the proposed vectorized implementation makes clear-sky priors computationally practical at scale, enabling

their use during both training and inference for long-horizon forecasting.

**Table 6: Variables from ERA5 and Baguan used for training and inference in Baguan-solar.**

Type	Variable name	Abbrev.	Stage1 input	Stage2 input	Levels
Single	low cloud cover	LCC	✓		-
Single	total cloud cover	TCC	✓		-
Single	total column water	TCW	✓	✓	-
Single	total column water vapour	TCWV	✓	✓	-
Single	total sky direct solar radiation at surface	FDIR	✓	✓	-
Single	surface solar radiation downwards	SSRD	✓	✓	-
Atmospheric	U wind component	U	✓		50, 250, 500, 600, 700, 850, 925
Atmospheric	V wind component	V	✓		50, 250, 500, 600, 700, 850, 925
Atmospheric	Temperature	T	✓		50, 250, 500, 600, 700, 850, 925
Atmospheric	Specific humidity	Q	✓	✓	50, 250, 500, 600, 700, 850, 925
Atmospheric	Geopotential	Z	✓		50, 250, 500, 600, 700, 850, 925